Bone Reports 18 (2023) 101668

Contents lists available at ScienceDirect

Bone Reports

journal homepage: www.elsevier.com/locate/bonr

FLNA-filaminopathy skeletal phenotypes are not due to an osteoblast autonomous loss-of-function

Emma M. Wade [a], Elizabeth A. Goodin [a], Yongqiang Wang [b], Tim Morgan [a], Karen E. Callon [c], Maureen Watson [c], Philip B. Daniel [a], Jillian Cornish [c], Christopher A. McCulloch [b], Stephen P. Robertson [a,*]

[a] Department of Women's and Children's Health, Dunedin School of Medicine, University of Otago, Dunedin, New Zealand
[b] Matrix Dynamics Group, Faculty of Dentistry, University of Toronto, Toronto, Ontario, Canada
[c] Bone and Joint Research Group, Department of Medicine, School of Medicine, The University of Auckland, Auckland, New Zealand

ARTICLE INFO

Keywords:
FLNA
Otopalatodigital Spectrum Disorders
Micro-CT
Mouse model

ABSTRACT

Mutations in *FLNA*, which encodes the cytoskeletal protein FLNA, cause a spectrum of sclerosing skeletal dysplasias. Although many of these genetic variants are recurrent and cluster within the gene, the pathogenic mechanism that underpins the development of these skeletal phenotypes is unknown. To determine if the skeletal dysplasia in *FLNA*-related conditions is due to a cell-autonomous loss-of-function localising to osteoblasts and/or osteocytes, we utilised mouse models to conditionally remove *Flna* from this cellular lineage. *Flna* was conditionally knocked out from mature osteocytes using the *Dmp1*-promoter driven Cre-recombinase expressing mouse, as well as the committed osteoblast lineage using the *Osx*-Cre or *Col1a1*-Cre expressing lines. We measured skeletal parameters with μCT and histological methods, as well as gene expression in the mineralised skeleton. We found no measureable differences between the conditional *Flna* knockout mice, and their control littermate counterparts. Moreover, all of the conditional *Flna* knockout mice, developed and aged normally. From this we concluded that the skeletal dysplasia phenotype associated with pathogenic variants in *FLNA* is not caused by a cell-autonomous loss-of-function in the osteoblast-osteocyte lineage, adding more evidence to the hypothesis that these phenotypes are due to gain-of-function in *FLNA*.

1. Introduction

Rare genetic diseases that affect the skeleton have enabled the elucidation of the molecular pathways critical for the development and maintenance of the skeleton (Monroe et al., 2012; Van Dijk et al., 2011). Pathogenic variants in the X-linked gene *FLNA* cause a spectrum of osteosclerotic, skeletal dysplasias called the otopalatodigital spectrum disorders (OPDSDs) (Robertson et al., 2003; Wade et al., 2020). The skeletal dysplasia associated with the OPDSDs ranges in severity from mild (in otopalatodigital syndrome type 1), to severe and life-limiting in females with Melnick Needles syndrome or Digitocutaneous dysplasia (Wade et al., 2020). Generally these conditions are characterised by skull base sclerosis, rib and spine deformities, undermodelling of the diaphyses, metaphyses, metacarpals, metatarsals and phalanges, supraorbital ridges, hypertelorism, micrognathia and joint contractures (Robertson et al., 2006). A range of soft tissue defects are also found to varying degrees of severity across the spectrum including urinary tract defects, tracheal stenosis, structural heart defects, cleft palate, and propensity to keloid scar (Robertson et al., 2006; Wade et al., 2017; Fitzsimmons et al., 1982). Despite this diversity of clinical entities caused by mutations in *FLNA*, the pathophysiology of the skeletal manifestations of these disorders remains unexplained.

Since the discovery of *FLNA* variants, two further causative genes have been identified that cause an autosomal dominant form of frontometaphyseal dysplasia (FMD). Pathogenic variants in *MAP3K7* (MIM 602614) and *TAB2* (MIM 605101) cause FMD2 (MIM 617173) and FMD3 respectively (Wade et al., 2017; Wade et al., 2016). This is unique among the *FLNA*-filaminopathies as only FMD is known to exhibit locus heterogeneity. The discovery of other causative genes has provided clues as to the mechanism of disease, but the role of FLNA in skeletal development remains to be defined.

It is hypothesised that variants in *FLNA* that lead to skeletal dysplasia

* Corresponding author.
E-mail address: stephen.robertson@otago.ac.nz (S.P. Robertson).

https://doi.org/10.1016/j.bonr.2023.101668
Received 8 March 2022; Received in revised form 23 February 2023; Accepted 26 February 2023
Available online 28 February 2023

have a gain-of-function mechanism because they do not lead to reduced FLNA protein levels and the causative mutations, all of which are missense or small in-frame indels, are often recurrent and clustered within the gene (Robertson et al., 2006; Clark et al., 2009). Direct evidence to support this assertion, however, is lacking. Furthermore, *FLNA* loss-of-function is associated with a different phenotype, a neuronal migration disorder called periventricular nodular heterotopia. This condition manifests in female heterozygotes and is not associated with skeletal symptoms or signs. (Wade et al., 2020; Pelizzo et al., 2019; Fox et al., 1998). Since the loss-of-function phenotype in hemizygous males is embryonic lethal, a definitive determination over whether FLNA deficiency affects the skeleton has not been established.

FLNA encodes the actin-binding protein FLNA (Gorlin et al., 1990). FLNA has a diverse range of cellular roles (Popowicz et al., 2006) and has mechanoprotective and mechanosensing properties (Gardel et al., 2006; Glogauer et al., 1998; Shifrin et al., 2009). Maintenance of bone mineral density and bone structure in the mammalian skeleton relies on mechanical input (Bonewald, 2006) and conceivably the mechanosensing role of FLNA is perturbed by gain-of-function variants leading to osteosclerosis.

Knockout of *Flna* in male mice results in embryonic lethality before embryonic day 15.5. The embryos have severe cardiac structural defects, as well as disorganised vasculature (Feng et al., 2006; Hart et al., 2006). Because of this early lethality, it is necessary to employ a conditional knockout to study the effects of *Flna* knockout in the developing skeleton in males. A knock out of *Flna* specifically in fibroblast and osteoblast cells using a *Col1a1* cre recombinase was associated with no obvious changes to body size or health, although bone indices were not explicitly examined (Mezawa et al., 2016). A monocyte specific (*LysM* cre) knockout of *Flna* leads to the formation of fewer, smaller osteoclasts, with defective migration due to loss of activation of actin cytoskeleton regulators. This defect causes reduced overall bone remodeling, diminished osteoblast activity and ultimately mild, low turnover-osteoporosis (Leung et al., 2010).

In this study, we test the hypothesis that the osteosclerotic phenotypes observed in the OPDSDs are due to a cell-autonomous loss of Flna in the osteoblast lineage by utilising well established transgenic mice lines (Feng et al., 2006; Lu et al., 2007; Rodda and McMahon, 2006; Liu et al., 2004). We find that loss of *Flna* from osteoblasts or osteocytes has no effect on skeletal development in mice leading us to reject this hypothesis. Our data confirm that *FLNA*-related skeletal dysplasias are not a result of loss-of-function of *FLNA* in the osteoblastic lineage and is consistent with the proposal that these pathogenic variants are acting through a gain-of-function mechanism.

2. Materials and methods

2.1. Transgenic mouse lines

The $Flna^{fl/fl}$ (129S4/SvJae, Flnam1.1caw [B6 speed congenic]) and Osx^{Cre} (B6.Cg-Tg [Sp7-tTA,tet0-EGFP/cre]1Amc/J) mouse lines were sourced from The Jackson Laboratory (Bar Harbour, ME, USA). The $Dmp1^{Cre}$ (B6N.FVB-Tg [Dmp1-cre] 1 Jqfe/BwdJ) strain was obtained from Dr. Lynda Bonewald (University of Missouri, Kansas City, MO, USA). The $Flna^{fl/fl}$ line was crossed with the Osx^{Cre} or $Dmp1^{Cre}$ lines, to generate $Flna^{CKO/y}/Osx^{Cre+}$ or $Flna^{CKO/y}/Dmp1^{Cre+}$ hemizygote, conditional knockout mice, and Cre + littermate controls at the University of Otago (Dunedin, NZ). Animal experiments carried out at Otago were approved by the University of Otago Animal Ethics Committee (protocol numbers: 33/17, 18–14, 18–46 and 19–203). All animals were housed under standard conditions at the Biomedical Research Facility (University of Otago, Dunedin, NZ). The non-experimental Osx^{Cre+} animals were maintained on Doxycycline (Merck, Kenilworth, NJ, USA) at a dose rate of 1 mg/kg, to suppress transgene expression. Genotyping was performed using DNA extracted from proteinase-K digested ear notches using specific primers (Table S1) and AmpliTaq Gold (ThermoFisher Scientific, Waltham, MA, USA).

Because *Flna* is X-linked, only male animals were assessed in this study. Animals were sacrificed at 3, 9 or 18 months of age for skeletal analysis. Ten days prior to cull, the animals received a subcutaneous injection of calcein green (30 mg/kg, Merck), a further subcutaneous injection of Alizarin-3-methylamine-N,N-diacetic acid dyhydrate (20 mg/kg, Merck) was delivered three days before cull. Mice were sacrificed by anaesthetic overdose (pentobarbital, 100 mg/kg), cardiac puncture and cervical dislocation.

The $Col1^{Cre}$ (CD-1 Col1a1 3.6-Cre) line was obtained from Dr. Barbara Kream (University of Connecticut, Farmington, CT, USA). The $Flna^{fl/fl}$ line housed in Toronto was obtained from Dr. David Kwiatkowski (Harvard University, Cambridge, MA, USA). $Flna^{fl/fl}$ mice were crossed with $Col1^{Cre}$ mice at the University of Toronto, to generate $Flna^{CKO/y}/Col1a1^{Cre+}$ hemizygote, conditional knockout mice, alongside WT littermate controls. Animals were sacrificed at 3 months old for skeletal analysis. All animal experiments carried out in Toronto were reviewed and approved by the Animal Care Committee, Faculty of Medicine (University of Toronto).

2.2. Micro-computational tomography

Whole femora were fixed in 70 % ethanol, rehydrated in saline solution 24 h prior to scanning and scanned wrapped in fine tissue paper soaked in saline solution. The distal 4.5 mm portion of each femur was scanned using the SkyScan 1172 (Bruker, Aartselar, Belgium) as follows: source voltage 50 kV, current 201 μA, isotropic voxel size 5 μm, and a 0.5 mm aluminium filter. Lower resolution scans were taken for images for illustrative purposes only. Scans were reconstructed in NreconLocal (Bruker) and analysis of 3D indices of bone structure was carried out in CTAn (Bruker). Datasets were binarised using a global thresholding method. A user-defined reference slice in the metaphyseal growth plate was assigned to each dataset. For trabecular parameters a 1.5 mm region of interest was defined, 0.75 mm proximal to the reference slice. For cortical bone analysis, a 0.75 mm region of interest was defined 2.75 mm proximal to the reference slice. Volumes of interest for trabecular and cortical bone were defined via interpolation of operator drawn areas containing either exclusively trabecular or cortical bone. The trabecular volume of interest was drawn a few voxels away from the endocortical surface. Tissue mineral density was calibrated against the attenuation coefficients of two phantoms of known mineral content, scanned and reconstructed in the same manner as the bone samples.

2.3. Histological analysis

Whole femora were fixed in 70 % ethanol and subject to histological analysis following μCT scanning. Bones were cryo-protected in 30 % sucrose (PBS) and embedded in O.C.T (Tissue Tek, Sakura, CA, USA). 6 μm sections were cut after being stabilised with 4D 16(UF) Cryofilm-tape (Section Lab, Japan) according to (Dyment et al., 2016). Sections were mounted on positive charged glass slides with 1 % chitosan adhesive and either left unstained or stained with an anti-Flna primary antibody (custom rabbit polyclonal to human Flna repeat 10, epitope ERATAGEVGQFQVDC, manufactured by Mimotopes Australia). The sensitivity and specificity of this antibody were validated via Western blot on Flna null mouse embryonic fibroblasts and M2 cells, and on human embryonic kidney cell lysate transiently transfected with human FLNA or FLNB constructs, respectively (Fig. S1).

Sections were imaged on a BX53 upright microscope, and photographed with a DP80 camera and the cellSens Dimension software (all Olympus, Tokyo, Japan).

2.4. Gene expression analysis

Whole, marrow flushed femora were collected and homogenised using the Omni tissue homogeniser (Omni, Kennesaw, GA, USA) in

Trizol reagent (Ambion, Austin, TX, USA). RNA was extracted using the NucleoSpin RNA Plus extraction kit (Macherey-Nagel, Düren, Germany). RNA quality was confirmed with the Qubit RNA HS assay kit (Invitrogen, Carlsbad, CA, USA) and the Bioanalyzer RNA 6000 Nano kit (Agilent, Santa Clara, CA, USA). For qPCR analysis, RNA was primed with random primers and OligoDT and cDNA was prepared using the SuperScript III First-Strand Synthesis System (ThermoFisher Scientific). PCR was carried out on the LightCycler 480 (Roche, Basel, Switzerland) using the SYBR Green master mix (Roche). Gene expression was quantified relative to three housekeeping genes using the LightCycler 480 software (Roche) and the qBase+ software (Biogazelle, Ghent, Belgium).

3. Results

3.1. Flna-osteocyte knockout mice develop normally

Flna is mechanoprotective therefore we hypothesised that Flna has a key mechanosensing role in osteocytes, the mechanosensing cells of the skeleton (Santos et al., 2009). Accordingly, a floxed *Flna* allele (*Flna*$^{fl/fl}$, exons 3–7 flanked by LoxP sites) (Feng et al., 2006) was conditionally knocked out from the osteocyte lineage using a strain expressing Cre-recombinase under control of the *Dmp1* promoter (*Dmp1*^{Cre}) (Lu et al., 2007). Twelve week old, hemizygous knockout male mice were examined alongside Cre + littermate controls as confirmed by genotyping PCRs (Fig. 1A, n = 6 per group, Table S1).

Pups were born at expected Mendelian ratios. RNA extracted from marrow-flushed femora dissected from the *Flna*$^{CKO/y}$/*Dmp1*$^{Cre+}$ and respective controls was used for relative qPCR quantification of total *Flna* transcript. There was no difference in the amount of *Flna* expressed in either the *Dmp1*^{Cre} controls or the *Flna* knockout mice in agreement with data from Feng et al. who showed no reduction in *Flna* RNA (Fig. S2). However RT-PCR using primers that flank the conditionally deleted region (Table S1) in the *Flna* transcript demonstrated that small deletion products were present in the cDNA of conditional knockout animals. These products were absent in *Dmp1*^{Cre} littermate control cDNA and no large product was observed because of PCR conditions that prevented the amplification of large products. Sanger sequencing of these products (and the large WT product amplified under different conditions) confirmed the deletion of *Flna* exons 2–6 or 2–7 in the conditional knockout animals which would prevent a functional Flna protein from being translated (Fig. S2). Furthermore, assessment of protein via immunohistochemistry (IHC) demonstrated loss of Flna from osteocytes in the femora of *Flna*$^{CKO/y}$/*Dmp1*$^{Cre+}$ mice (Figs. 1B, S3). There were no apparent phenotypic differences between the *Flna*$^{CKO/y}$/*Dmp1*$^{Cre+}$ animals and their respective Cre + littermate controls. Mice were aged to 18 months and the *Flna*$^{CKO/y}$/*Dmp1*$^{Cre+}$ animals tended to be longer and heavier than their Cre + littermate controls, but this did not reach significance (Fig. S4). No health issues specific to the *Flna*$^{CKO/y}$/*Dmp1*$^{Cre+}$ animals emerged.

3.2. Skeletal manifestations of *Flna*$^{CKO/y}$/*Dmp1*$^{Cre+}$ mice

The OPD spectrum skeletal phenotype manifests as osteosclerosis in the long bones (Robertson et al., 2006; Gorlin and Cohen, 1969). To investigate if loss of Flna, in osteocytes, causes a skeletal phenotype, we analysed the long bones of 3-month old *Flna*$^{CKO/y}$/*Dmp1*$^{Cre+}$ mice. Micro-computed tomography (μCT) was used to scan the distal femur of *Flna*-knockout male mice and littermate controls at a resolution of 5 μm. Standard parameters of trabecular architecture were measured as recommended by (Bouxsein et al., 2010). When assessing bone volume fraction (BV/TV), trabecular thickness (Tb.Th), trabecular number (Tb.N), and trabecular separation (Tb.Sp) we found no significant differences between *Flna*$^{CKO/y}$/*Dmp1*$^{Cre+}$ mice and their littermate controls (p = 0.53, 0.51, 0.61 and 0.50 respectively, unpaired t-test) (Fig. 1C and D, Table S2). Cortical architecture was also assessed using recommended guidelines from (Bouxsein et al., 2010), and we found no significant differences in 3D measures of total cross-sectional area (Tt.Ar), cortical bone area (Ct.Ar), cortical area fraction (Ct.Ar/Tt.Ar), and average cortical thickness (Ct.Th) between *Flna*$^{CKO/y}$/*Dmp1*$^{Cre+}$ mice and their littermate controls (p = 0.92, 0.53, 0.33 and 0.35 respectively, unpaired t-test) (Fig. 1D, Table S2). Furthermore we found no significant difference in the percentage of pores in the cortical fraction (p = 0.16) or the tissue mineral density (TMD) (p = 0.13) between *Flna*$^{CKO/y}$/*Dmp1*$^{Cre+}$ and littermate controls (Table S2).

RNA was extracted from marrow-flushed, whole femur and qPCR was used to quantify markers of osteoblastogenesis and bone mineralisation. There were no gene expression differences between *Flna*$^{CKO/y}$/*Dmp1*$^{Cre+}$ bones and those from littermate controls, including late-stage markers of mineralisation or osteocyte specific genes such as *Alpl, Dmp1* and *Ibsp* (Fig. 1E). Calculations of mineralising surface, bone formation rate and mineral apposition rate taken from calcein and alizarin stained bone cryo-sections also showed no significant difference (n = 3 per group, p = 0.77, 0.22 and 0.12 respectively, Table 1). Because of the lack of skeletal manifestations, and the osteocyte-specific nature of this knockout, it was deemed unnecessary to analyse the osteoclast phenotype in these animals. Although these data indicate that loss of Flna from the mechanosensing cells of the skeleton does not result in osteosclerosis, it is possible that absence of *Flna* from the osteocytes over the lifespan could be significant because of the known role of Flna in cellular mechanoprotection. *Flna*$^{CKO/y}$/*Dmp1*$^{Cre+}$ mice alongside their Cre + littermate controls were aged to 18 months (n = 6 per group) and their femora were assessed by μCT. The same, standard parameters of trabecular and cortical architecture were calculated and we found no significant differences, at the 95 % confidence interval, in the 3D structure of the trabecular bone, or in the 3D structure, porosity or TMD of the cortical compartment (Fig. 2A and B, Table S2). We therefore found no changes to the appendicular skeleton when *Flna* was removed from osteocytes. This adds to the evidence that the pathogenic variants in *FLNA* that cause OPDSDs do not mediate their effects through loss-of-function in this cell type. However, it is possible that a more widespread deficiency over the osteoblastic-osteocytic lineage could mediate such an effect.

3.3. Knockout of Flna from the osteoblast lineage

An osteoblast-specific knockout of *Flna* was created by crossing *Flna*$^{fl/fl}$ mice with a Cre-recombinase expressing strain under the control of the *Sp7* promoter (*Osx*^{Cre}) (Rodda and McMahon, 2006). Flna conditional knockout was confirmed by genotyping PCRs as before (Fig. 3A, Table S1). As in the *Flna*$^{CKO/y}$/*Dmp1*$^{Cre+}$ mice, no reduction in *Flna* transcript was seen in marrow-flushed *Flna*$^{CKO/y}$/*Osx*$^{Cre+}$ femora (Fig. S2). However the conditional knockout deletion products were present in the cDNA of these animals when analysed via RT-PCR, confirming that a functional Flna protein could not be translated in the CKO cells (Fig. S2, Table S1). Furthermore, IHC showed loss of Flna from osteocytes in the femora of *Flna*$^{CKO/y}$/*Osx*$^{Cre+}$ mice (Figs. 3B, S3).

In the litters of the *Flna*^{CKO} x *Osx*^{Cre} cross there was a trend towards reduced offspring that carried the Cre transgene, however this did not reach significance (272 offspring assessed, X^2 = 7.37, 3 degrees of freedom, p = 0.061). Furthermore it has previously been reported that *Osx*^{Cre} mice have reduced growth (Walkley et al., 2008), therefore we included the Cre in the littermate controls for this cross. Malocclusion was a feature of both the *Flna*$^{CKO/y}$/*Osx*$^{Cre+}$ knockout and the Cre + controls, as previously reported (Walkley et al., 2008). Animals in this line were therefore aged to 9 months before malocclusion caused significant welfare issues. No other health problems, specific to the *Flna* knockout mice, were observed and *Flna*$^{CKO/y}$/*Osx*$^{Cre+}$ mice maintained comparable growth parameters to the Cre + littermate controls over the 9 months (Fig. S4).

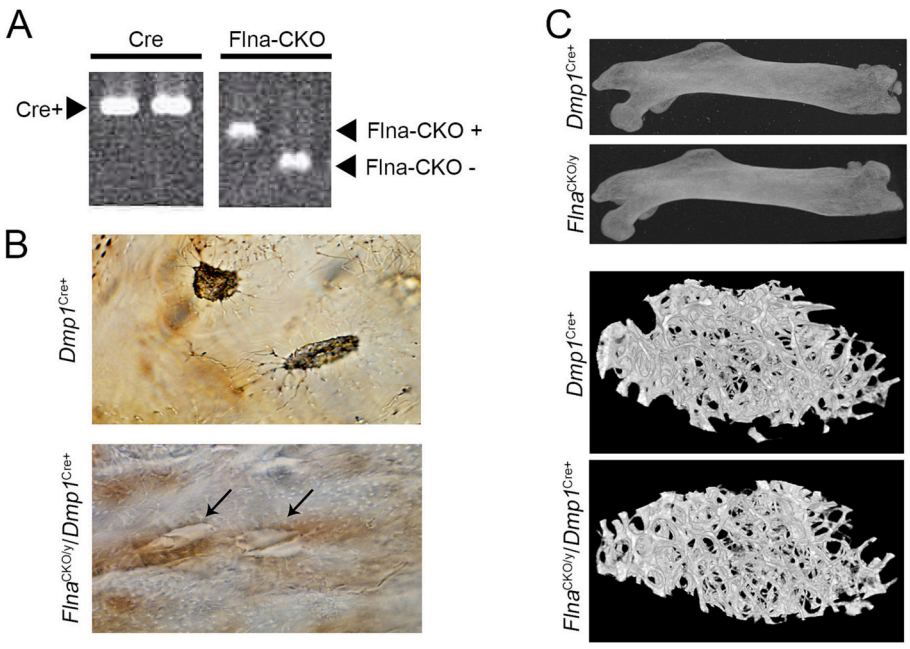

Fig. 1. Flna knockout in the osteocyte cell compartment of 3 month old male mice. (A) Example of genotyping PCRs performed on DNA extracted from ear notch biopsies. Cre and Flna-CKO PCRs carried out on same two animals to show presence of the Cre recombinase gene in all animals studied and presence or absence of Flna-CKO. (B) Flna immunohistochemistry (IHC) on femora cryo-sections taken from Flna in *Flna*$^{CKO/y}$/*Dmp1*$^{Cre+}$ mice and Cre + littermate controls (black arrows point to osteocytes). (C) Images taken from μCT scans of distal femur in 3 month old *Flna*$^{CKO/y}$/*Dmp1*$^{Cre+}$ mice and Cre + littermate controls.(D) Quantification of trabecular and cortical parameters measured by μCT in 3 month old *Flna*$^{CKO/y}$/*Dmp1*$^{Cre+}$ mice and Cre + littermate controls ($n = 6$ per group). % BV/TV – trabecular bone volume fraction, Tb.N – trabecular number, Tt.Ar – total cortical cross-sectional area, Ct.Th – average cortical thickness (E) qPCR analysis of key osteogenic genes performed on RNA extracted from mineralised femora of *Flna*$^{CKO/y}$/*Dmp1*$^{Cre+}$ mice and Cre + littermate controls (n = 6 per group).

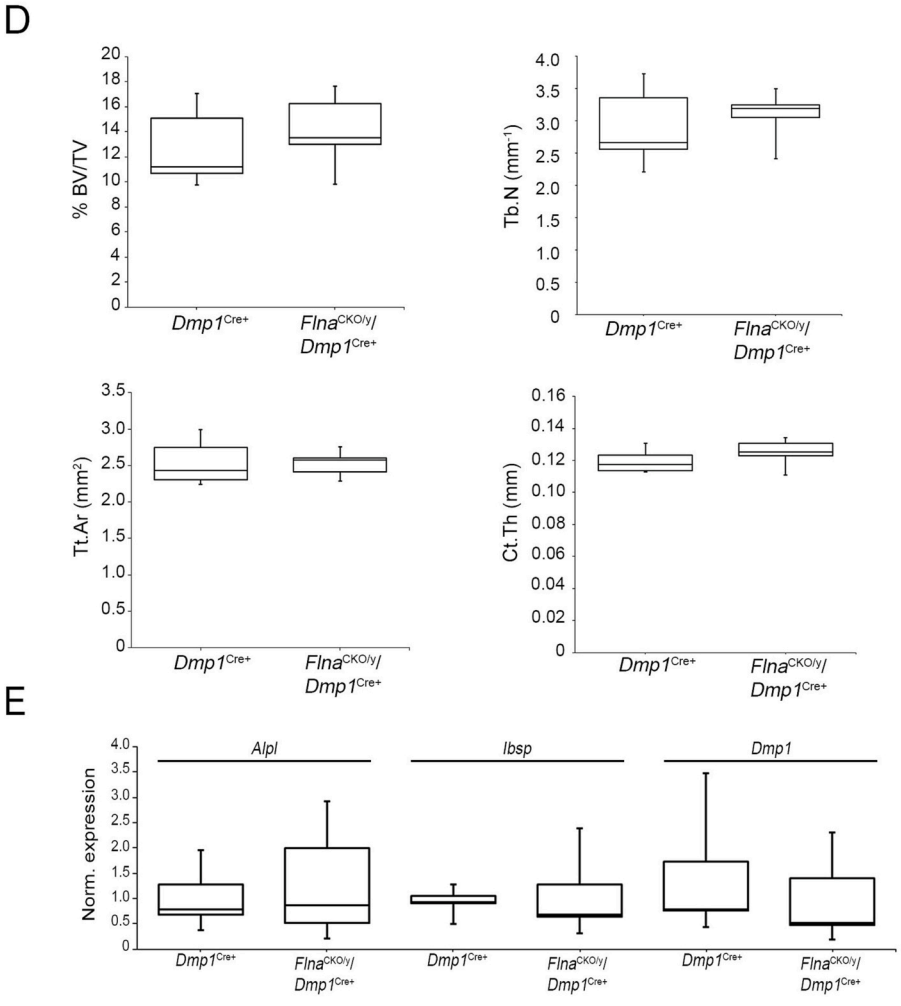

Table 1
Mineralising surface, mineral apposition rate and bone formation rate in 3 month old *Flna*$^{CKO/y}$/*Dmp1*$^{Cre+}$ and *Flna*$^{CKO/y}$/*Osx*$^{Cre+}$ mice and littermate controls.

Flna$^{CKO/y}$/*Dmp1*$^{Cre+}$	3 months		
	Flna$^{CKO/y}$/*Dmp1*$^{Cre+}$	*Dmp1*$^{Cre+}$	*P* value
Mineralising surface (%)	23.49 ± 3.18	22.55 ± 3.29	0.767
Mineral apposition rate (μm/day)	1.391 ± 0.068	2.376 ± 0.855	0.118
Bone formation rate (μm/day)	0.329 ± 0.061	0.564 ± 0.271	0.221

Flna$^{CKO/y}$/*Osx*$^{Cre+}$	3 months		
	Flna$^{CKO/y}$/*Osx*$^{Cre+}$	*Osx*$^{Cre+}$	*P* value
Mineralising surface (%)	21.61 ± 5.26	13.76 ± 5.01	0.135
Mineral apposition rate (μm/day)	1.537 ± 0.210	1.554 ± 0.295	0.938
Bone formation rate (μm/day)	0.328 ± 0.058	0.223 ± 0.125	0.259

3.4. Skeletal manifestations of the *Flna*$^{CKO/y}$/*Osx*$^{Cre+}$ mice

Whole femora were collected from 3-month old *Flna*$^{CKO/y}$/*Osx*$^{Cre+}$ mice and Cre + littermate controls ($n = 6$ per group). μCT was used to scan the distal femur at a resolution of 5 μm. The same range of standard, architectural trabecular parameters were measured as for the *Flna*$^{CKO/y}$/*Dmp1*$^{Cre+}$ mice. No differences in BV/TV ($p = 0.46$), Tb.Th ($p = 0.67$), Tb.N ($p = 0.27$), and Tb.Sp ($p = 0.15$) were found in *Flna*$^{CKO/y}$/*Osx*$^{Cre+}$ compared to Cre + littermate controls (Fig. 3C, Table S2). Again, no differences were found in structural parameters of cortical bone including Tt.Ar ($p = 0.29$), Ct.Ar ($p = 0.16$), Ct.Ar/Tt.Ar ($p = 0.96$), and Ct.Th ($p = 0.48$) between *Flna*$^{CKO/y}$/*Osx*$^{Cre+}$ and Cre + littermate controls (Table S2). Expression of a selection of osteoblast- and osteoclast-specific genes was measured in total femoral RNA via qPCR. No statistically significant differences in expression of any of the genes measured were noted (Fig. 3E). Furthermore, we measured mineralising surface, bone formation rate and mineral apposition rate from calcein and alizarin stained femora cryo-sections ($n = 3$ per group, $p = 0.13$, 0.26 and 0.94 respectively) and found no significant differences in any measure of bone accrual between the *Flna*$^{CKO/y}$/*Osx*$^{Cre+}$ mice and their Cre + counterparts (Table 1).

To understand if loss of *Flna* from the osteoblast lineage altered how the skeleton adapted to mechanical stress over a lifetime, we aged the *Flna*$^{CKO/y}$/*Osx*$^{Cre+}$ male mice to 9 months old. Comparisons at older ages were precluded due to the high incidence of malocclusion in the *Osx*$^{Cre+}$ mice. Advanced age did not manifest a long bone phenotype as we found no significant difference in any of the standard trabecular or cortical architectural parameters measured via μCT at the 9 month timepoint (Fig. 3D, Table S2).

3.5. Skeletal manifestations in *Flna*$^{CKO/y}$/*Col1*$^{Cre+}$ mice

To further validate our observations in mice with Flna deleted within the osteoblast linage, we examined the skeletal phenotype of another *Flna* conditional knockout mouse, albeit with lesser tissue specificity and a later developmental timepoint for cre-lox excision, than Osx-cre. The *Col1*^{Cre} mouse strain (Liu et al., 2004) was used to conditionally knockout *Flna* from fibroblasts and osteoblasts as previously reported by Mezawa et al (Mezawa et al., 2016) (Fig. S2). μCT was used to scan the distal femur from 3-month old *Flna*$^{CKO/y}$/*Col1*$^{Cre+}$ mice alongside WT littermate controls ($n = 4$ per group). Similar to the *Flna*$^{CKO/y}$/*Osx*$^{Cre+}$ mice, we found no significant differences in any of the standard measurements of trabecular or cortical structural parameters (Fig. 3E,

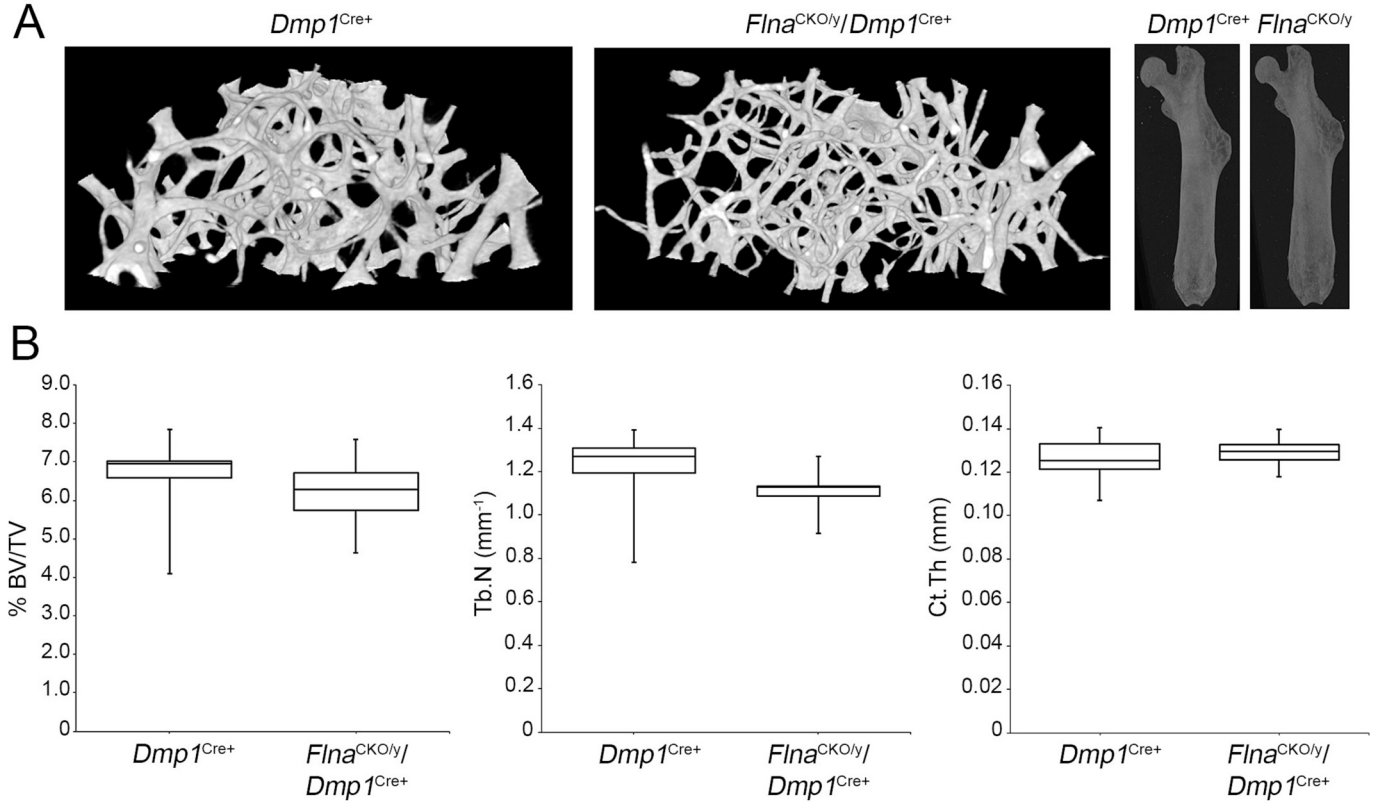

Fig. 2. Flna knockout from the osteocyte compartment of 18 month old male mice. (A) Images taken from μCT scans of the distal femur in 18 month old *Flna*$^{CKO/y}$/*Dmp1*$^{Cre+}$ mice and Cre + littermate controls. (B) Quantification of trabecular and cortical parameters measured by μCT scan ($n = 6$ per group). % BV/TV – trabecular bone volume fraction, Tb.N – trabecular number, Ct.Th – average cortical thickness.

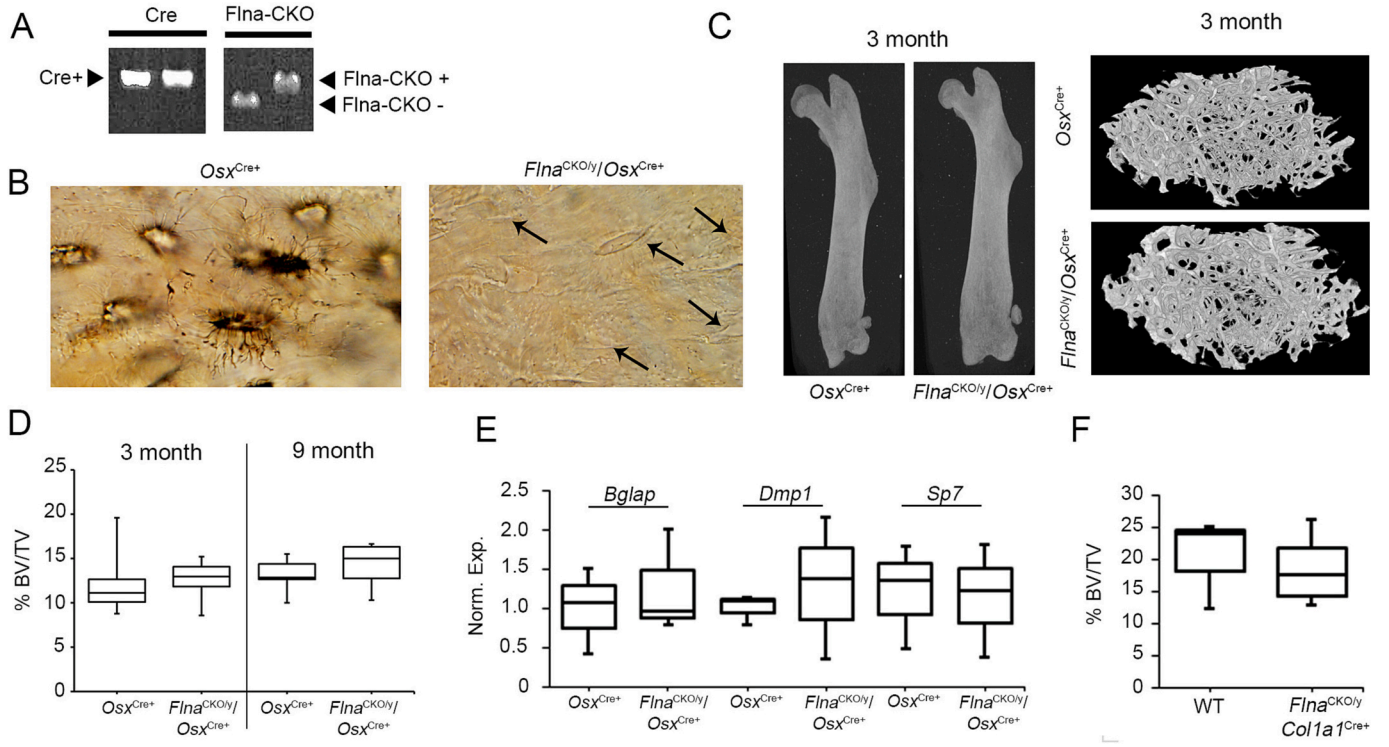

Fig. 3. Flna knockout from the established osteoblast lineage in 3 month old male mice. (A) Example genotyping PCRs performed on DNA extracted from ear notch biopsies. Cre and Flna-CKO PCRs carried out on same two animals. (B) Flna IHC undertaken on cryo-sections of femora taken from *Flna*$^{CKO/y}$/*Osx*$^{Cre+}$ mice and Cre + littermate controls (arrows show osteocytes). (C) Representative images taken from μCT of the femur of 3 month old *Flna*$^{CKO/y}$/*Osx*$^{Cre+}$ mice and Cre + littermate controls. (D) Quantification of trabecular bone volume fraction (% BV/TV) measured from μCT scans in *Flna*$^{CKO/y}$/*Osx*$^{Cre+}$ mice and Cre + littermate controls (n = 6 per group). (E) Gene expression analysis using RNA extracted from mineralised long bone in *Flna*$^{CKO/y}$/*Osx*$^{Cre+}$ mice and Cre + littermate controls (n = 6 per group). (E) Quantification of trabecular BV/TV measured from μCT scans of *Flna*$^{CKO/y}$/*Col1a1*$^{Cre+}$ femora and WT littermate controls (*n* = 4 per group).

Table S2), confirming that removal of *Flna* from the osteoblast lineage does not result in the osteosclerotic phenotype seen in the OPD spectrum disorders.

4. Discussion

A large number of missense variants in the X-linked gene *FLNA* that do not alter the stability or level of the protein cause a spectrum of skeletal dysplasias called the OPDSDs (Robertson et al., 2003; Wade et al., 2020; Clark et al., 2009). Although the level of FLNA is preserved in non-skeletal tissue in these conditions (Robertson et al., 2006; Wade et al., 2021), it is unclear if a specific deficit is conferred by these mutations in bone. This is one hypothesis to explain the predominantly skeletal presentation of a disorder caused by mutations in a near ubiquitously expressed gene (Gerrard et al., 2016). This specific deficit could conceivably be conferred by a loss- or a gain-of-function mechanism.

A gain-of-function mechanism has been proposed previously because (a) the mutations in *FLNA* are both recurrent and clustered (Wade et al., 2020), (b) loss-of-function pathogenic variants in *FLNA* cause a separate neurological and connective tissue disorder with no skeletal abnormalities in female heterozygotes (Parrini et al., 2006) as well as in rare hemizygous males with reduced *FLNA* expression (Oda et al., 2016), and (c) two further FMD-causing genes act through a gain-of-function mechanism suggesting there may be a shared pathway in the pathogenesis of the OPDSDs that is inappropriately activated by variants in *FLNA, MAP3K7* or *TAB2*. This is further supported by the in-vitro evidence that one FMD mutation causes FLNA hyper-phosphorylation (Ithychanda et al., 2017). Reflecting the possible loss- and gain-of-function duality in *FLNA,* loss-of-function pathogenic variants in *MAP3K7* or *TAB2* convey different phenotypes - cardiospondylocarpofacial syndrome and a recognisable phenotype of cardiac and connective tissue abnormalities respectively (Le Goff et al., 2016; Engwerda et al., 2021). However clinical or pathological study of the skeleton from individuals with *FLNA* loss-of-function alleles is precluded by the embryonic lethality conferred by such alleles in males.

To mitigate the issue that complete knockout of *Flna* is lethal, and to question if the skeletal phenotype of the OPDSDs is caused by a deficiency of *FLNA* in the skeleton, we utilised a conditional *Flna* knockout. A limitation of this study was our ability to robustly demonstrate loss of FLNA protein from the cells of interest. However we utilised previously well-characterised conditional knockout and cre-recombinase expressing mouse lines, and showed evidence of *Flna* recombination at the genomic and transcript levels. There are two main cellular linages in the bone, osteoblasts and osteoclasts. An osteoclast-specific knockout of *Flna* has been investigated, and it did not recapitulate the skeletal dysplasia of the OPDSDs (Leung et al., 2010). Therefore, we investigated the consequences of removing *Flna* from the other major skeletal lineage, the osteoblast. Despite the role of Flna in cellular mechanosensing (Gardel et al., 2006), and the importance of the osteocyte in the mechano-response of the skeleton (Bonewald, 2006), we observed no phenotype in the osteocyte-specific knockout *Flna* mice. Whilst this finding adds to the evidence that pathogenic *FLNA* variants that cause the OPDSDs are gain-of-function, it is nevertheless intriguing that loss of an almost-ubiquitously expressed, essential cytoskeletal and signaling protein has no effect on the development of the skeleton when knocked out in osteocytes. In order to further elucidate if Flna has a role in skeletal development, and specifically bone anabolism, we conditionally knocked out *Flna* from the entire osteoblastic lineage. Once again, we did not observe a skeletal phenotype when *Flna* was removed from the osteoblasts using either the *Osx*- or *Col1*-promoter driven Cre lines.

In the *Flna*-KO mouse some abnormalities of the skeleton were described in embryos (E15.5). The sternum fails to fuse in hemizygous

males and delayed fusion also occurs in heterozygous females with some deformities in the resulting adult sternum (Hart et al., 2006). We observed no fusion problems in the sterna of the osteocyte or osteoblast *Flna* knockout mice. The complete *Flna* knockout mice also commonly exhibit a cleft palate (Hart et al., 2006), another phenotype we did not observe in the mice studied here. Both these phenotypes are caused by defects in the cells that precede the appearance of mature, mineralised bone, in this instance the cartilage of the developing axial skeleton and the migrating neural crest cells of the facial appendages. Consequently, it is not surprising that we did not recapitulate these phenotypes with our *Flna* knockout which only targeted the cells of the mature skeleton.

Conceivably, FLNA is not essential for the function and maturation of osteoblasts, and loss of filamin from these cells therefore has no measurable effect on the skeleton. However, it is plausible that earlier in skeletal development, in both mice and humans, Flna is critical for the movement and migration of progenitor cells as they form pre-mineralised skeletal structures (Baldassarre et al., 2009), leading to some of the skeletal defects observed in the *Flna*-knockout mouse. Consistent with this proposition, a cellular migratory defect is seen in *Flna*-knockout osteoclasts (Leung et al., 2010).

In conclusion, we have shown that knockout of *Flna* from mouse osteocytes, as well as the osteoblast lineage results in no measurable changes to the mature skeleton. This adds to the evidence that the pathogenic variants in *FLNA* that result in the OPD spectrum of disorders likely operate through a gain-of-function mechanism or show that Flna has no function in the mature mouse osteoblast.

CRediT authorship contribution statement

E Wade – project management, practical work, manuscript writing; L Goodin, Y Wang, P Daniel, T Morgan – animal management, practical work; K Cullon, M Watson, J Cornish – training, technical oversight, C McCulloch – provision of the $Flna^{CKO/y}/Col1a1^{Cre=}$ mice, S Robertson – conceptualisation, manuscript writing, group management.

Declaration of competing interest

The authors have no conflicts of interest to declare.

Data availability

No data was used for the research described in the article.

Acknowledgements

We thank the Histology Service (Otago Micro- and Nano-scale Imaging Unit), Otago University, for their help with the histological analysis.

Funding

EW and PD were funded by the Royal Society of New Zealand, Marsden Fund. EW and SR received funding from Cure Kids New Zealand. CAM is supported by a Canada Research Chair and by CIHR Operating grant MOP-503020.

Appendix A. Supplementary data

Supplementary data to this article can be found online at https://doi.org/10.1016/j.bonr.2023.101668.

References

Baldassarre, M., Razinia, Z., Burande, C., Lamsoul, I., Lutz, P., Calderwood, D., 2009. Filamins regulate cell spreading and initiation of cell migration. PLoS ONE. 4, e7830.
Bonewald, L., 2006. Mechanosensation and transduction in osteocytes. BoneKEy-Osteovision 3, 7–15.
Bouxsein, M., Boyd, S., Christiansen, B., Guldberg, R., Jepsen, K., Muller, R., 2010. Guidelines for assessment of bone microstructure in rodents using micro-computed tomography. J. Bone Miner. Res. 25, 1468–1486.
Clark, A., Sawyer, G., Robertson, S., Sutherland-Smith, A., 2009. Skeletal dysplasias due to filamin a mutations result from a gain-of-function mechanism distinct from allelic neurological disorders. Hum. Mol. Genet. 18, 4791–4800.
Dyment, N.A., Jiang, X., Chen, L., Hong, S.-H., Adams, D.J., Ackert-Bicknell, C., et al., 2016. High-throughput, multi-image cryohistology of mineralized tissues. JoVE 14, e54468.
Engwerda, A., Leenders, E.K.S.M., Frentz, B., Terhal, P.A., Löhner, K., de Vries, B.B.A., et al., 2021. TAB2 deletions and variants cause a highly recognisable syndrome with mitral valve disease, cardiomyopathy, short stature and hypermobility. Eur. J. Hum. Genet. 29, 1669–1676.
Feng, Y., Chen, M., Moskowitz, I., Mendonza, A., Vidali, L., Nakamura, F., et al., 2006. Filamin A (FLNA) is required for cell-cell contact in vascular development and cardiac morphogenesis. Proceedings of the National Academy of Sciences. 103, 19836–19841.
Fitzsimmons, J., Fitzsimmons, E., Barrow, M., Gilbert, G., 1982. Fronto-metaphyseal dysplasia. Further delineation of the clinical syndrome. Clin Genet. 22, 195–205.
Fox, J., Lamperti, E., Eksioglu, Y., Hong, S., Feng, Y., Graham, A., et al., 1998. Mutations in filamin 1 prevent migration of cerebral cortical neurons in human periventricular heterotopia. Neuron 21, 1315–1325.
Gardel, M., Nakamura, F., Hartwig, J., Crocker, J., Stossel, T., Weitz, D., 2006. Prestressed F-actin networks cross-linked by hinged filamins replicate mechanical properties of cells. PNAS 103, 1762–1767.
Gerrard, D.T., Berry, A.A., Jennings, R.E., Piper Hanley, K., Bobola, N., Hanley, N.A., 2016. An integrative transcriptomic atlas of organogenesis in human embryos. elife 5, e15657.
Glogauer, M., Arora, P., Chou, D., Janmey, P., Downey, G., McCulloch, C., 1998. The role of actin-binding protein 280 in integrin-dependent mechanoprotection. J. Biol. Chem. 273, 1689–1698.
Gorlin, R., Cohen, M.J., 1969. Frontometaphyseal dysplasia. A new syndrome. American Journal of Diseases of Children. 118, 487–494.
Gorlin, J., Yamin, R., Egan, S., Stewart, M., Stossel, T., Kwiatkowski, D., et al., 1990. Human endothelial actin-binding protein (ABP-280, nonmuscle filamin): a molecular leaf spring. J. Cell Biol. 111, 1089–1105.
Hart, A., Morgan, J., Schneider, K., McKie, L., Bhattacharya, S., Jackson, I., et al., 2006. Cardiac malformations and midline skeletal defects in mice lacking filamin A. Hum. Mol. Genet. 15, 2457–2467.
Ithychanda, S., Dou, K., Robertson, S., Qin, J., 2017. Structural and thermodynamic basis of a frontometaphyseal dysplasia mutation in filamin A. J. Biol. Chem. 292, 8390–8400.
Le Goff, C., Rogers, C., Le Goff, W., Pinto, G., Bonnet, D., Chrabieh, M., et al., 2016. Heterozygous mutations in MAP3K7, encoding TGF-β-activated kinase 1, cause cardiospondylocarpofacial syndrome. Am. J. Hum. Genet. 99, 407–413.
Leung, R., Wang, Y., Cuddy, K., Sun, C., Magalhaes, J., Grynpas, M., et al., 2010. Filamin a regulates monocyte migration through rho small GTPases during osteoclastogenesis. J. Bone Miner. Res. 25, 1077–1091.
Liu, F., Woitge, H.W., Braut, A., Kronenberg, M.S., Lichtler, A.C., Mina, M., Kream, B.E., et al., 2004. Expression and activity of osteoblast-targeted Cre recombinase transgenes in murine skeletal tissues. Int. J. Dev. 48, 645–653.
Lu, Y., Xie, Y., Zhang, S., Dusevich, V., Bonewald, L., Feng, J., 2007. DMP1-targeted cre expression in odontoblasts and osteocytes. J. Dent. Res. 86, 320–325.
Mezawa, M., Pinto, V.I., Kazembe, M.P., Lee, W.S., McCulloch, C.A., 2016. Filamin a regulates the organization and remodeling of the pericellular collagen matrix. FASEB J. 30, 3613–3627.
Monroe, D., McGee-Lawrence, M., Oursler, M., Westendorf, J., 2012. Update on wnt signalling in bone cell biology and bone disease. Gene 492, 1–18.
Oda, H., Sato, T., Kunishima, S., Nakagawa, K., Izawa, K., Hiejima, E., et al., 2016. Exon skipping causes atypical phenotypes associated with a loss-of-function mutation in FLNA by restoring its protein function. Eur. J. Hum. Genet. 24, 408–414.
Parrini, E., Ramazzotti, A., Dobyns, W., Mei, D., Moro, F., Veggiotti, P., et al., 2006. Periventricular heterotopia: phenotypic heterogeneity and correlation with filamin a mutations. Brain 129, 1892–1906.
Pelizzo, G., Collura, M., Puglisi, A., Pappalardo, M.P., Agolini, E., Novelli, A., et al., 2019. Congenital emphysematous lung disease associated with a novel filamin a mutation. Case report and literature review. BMC Pediatr. 19, 86.
Popowicz, G., Schleicher, M., Noegel, A., Holak, T., 2006. Filamins: promiscuous organizers of the cytoskeleton. Trends Biochem. Sci. 31, 411–419.
Robertson, S., Twigg, S., Sutherland-Smith, A., Biancalana, V., Gorlin, R., Horn, D., et al., 2003. Localized mutations in the gene encoding the cytoskeletal protein filamin a cause diverse malformations in humans. Nat. Genet. 33, 487–491.
Robertson, S., Jenkins, Z., Morgan, T., Ades, L., Aftimos, S., Boute, O., et al., 2006. Frontometaphyseal dysplasia: mutations in FLNA and phenotypic diversity. Am. J. Med. Genet. A 140, 1726–1736.
Rodda, S., McMahon, A., 2006. Distinct roles for hedgehog and canonical wnt signaling in specification, differentiation and maintenance of osteoblast progenitors. Development 133, 3231–3244.
Santos, A., Bakker, A., Klein-Nulend, J., 2009. The role of osteocytes in bone mechanotransduction. Osteoporos. Int. 20, 1027–1031.
Shifrin, Y., Arora, P., Ohta, Y., Calderwood, D., McCulloch, C., 2009. The role of FilGAP-filamin a interactions in mechanoprotection. Mol. Biol. Cell 20, 1269–1279.
Van Dijk, F., Cobben, J., Kariminejad, A., Maugeri, A., Nikkels, P., van Rijn, R., et al., 2011. Osteogenesis imperfecta: a review with clinical examples. Mol. Syndromol. 2, 1–20.

Wade, E.M., Daniel, P., Jenkins, Z., McInerney-Leo, A., Leo, P., Morgan, T., et al., 2016. Mutations in MAP3K7 that alter the activity of the TAK1 signaling complex cause frontometaphyseal dysplasia. Am. J. Hum. Genet. 99, 392–406.
Wade, E.M., Jenkins, Z., Daniel, P., Morgan, T., Addor, M., Ades, L., et al., 2017. Autosomal dominant frontometaphyseal dysplasia: delineation of the clinical phenotype. Am. J. Med. Genet. Part A 173, 1739–1746.
Wade, E.M., Halliday, B.J., Jenkins, Z.A., O'Neill, A.C., Robertson, S.P., 2020. The X-linked filaminopathies: synergistic insights from clinical and molecular analysis. Hum. Mutat. 41, 865–883.
Wade, E.M., Jenkins, Z.A., Morgan, T., Gimenez, G., Gibson, H., Peng, H., et al., 2021. Exon skip-inducing variants in FLNA in an attenuated form of frontometaphyseal dysplasia. Am. J. Med. Genet. A 185, 3675–3682.
Walkley, C., Qudsi, R., Sankaran, V., Perry, J., Gostissa, M., Roth, S., et al., 2008. Conditional mouse osteosarcoma, dependent on p53 loss and potentiated by loss of rb, mimics the human disease. Genes Dev. 22, 1662–1676.